Hot-Carrier Dynamics and Chemistry in Dielectric Polymers

Hiroyuki Kumazoe,[†] Shogo Fukushima,[†] Subodh Tiwari,[‡] Chiho Kim,[§] Tran Doan Huan,[§]
Rajiv K. Kalia,[‡] Aiichiro Nakano,*[,‡] Rampi Ramprasad,[§] Fuyuki Shimojo,[†] and Priya Vashishta[‡]

[†]Department of Physics, Kumamoto University, Kumamoto 860-8555, Japan
[‡]Collaboratory for Advanced Computing and Simulations, University of Southern California, Los Angeles, California 90089-0242, United States
[§]School of Materials Science and Engineering, Georgia Institute of Technology, Atlanta, Georgia 30332, United States

Ⓢ *Supporting Information*

ABSTRACT: Dielectric polymers are widely used in electronics and energy technologies, but their performance is severely limited by the electrical breakdown under a high electric field. Dielectric breakdown is commonly understood as an avalanche of processes such as carrier multiplication and defect generation that are triggered by field-accelerated hot electrons and holes. However, how these processes are initiated remains elusive. Here, nonadiabatic quantum molecular dynamics simulations reveal microscopic processes induced by hot electrons and holes in a slab of an archetypal dielectric polymer, polyethylene, under an electric field of 600 MV/m. We found that electronic-excitation energy is rapidly dissipated within tens of femtoseconds because of strong electron−phonon scattering, which is consistent with quantum-mechanical perturbation calculations. This in turn excites other electron−hole pairs to cause carrier multiplication. We also found that the key to chemical damage is localization of holes that travel to a slab surface and weaken carbon−carbon bonds on the surface. Such quantitative information can be incorporated into first-principles-informed, predictive modeling of dielectric breakdown.
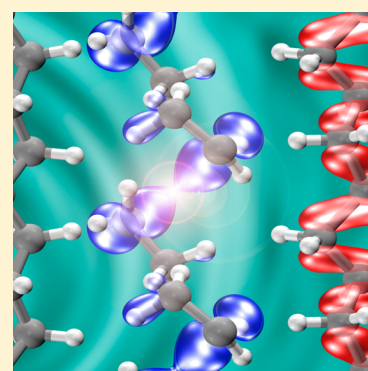
Advancement of energy-storage and pulsed-power technologies[1−4] is severely limited by the breakdown of dielectric materials under high electric field.[5,6] Predictive theory and mechanistic understanding are indispensable for the mitigation of dielectric breakdown. Electronic theory of dielectric breakdown exists for inorganic crystalline solids,[7,8] starting with the pioneering works by Zener,[9] Frölich,[10] and von Hippel.[11] In the avalanche breakdown theory, the critical electric field for failure is calculated from the balance between the energy-gain rate due to field and energy-loss rate due to electron−phonon scattering. While no such theory exists to quantitatively predict the breakdown field in polymers, experimental observations suggest that dielectric breakdown in polymers is a positive feedback process. Here, injection of free charge carriers (i.e., electrons and holes), when accelerated under large applied electric field, triggers various processes such as carrier multiplication (i.e., excitation of secondary electron−hole pairs) and defect generation, which in turn promote further carrier activities. This positive feedback process eventually leads to electromechanical failure involving microstructural evolution such as cracks.[5,6] Among dielectric polymers, the most extensively studied for dielectric breakdown is polyethylene (PE),[12] which has unusual electronic properties such as negative electron affinity in its crystalline form.[13] Recent studies have shown important effects of chemical[14−17] and morphological[18−20] defects on the electronic structures (e.g., energy levels of electron and hole trap

states) of PE. However, how various dynamic processes (e.g., carrier multiplication and defect generation) are initiated by accelerated electrons and holes remains elusive.

In order to understand the elementary processes leading to breakdown in PE, we performed nonadiabatic quantum molecular dynamics (NAQMD) simulations of excited hot-carrier dynamics in PE under a uniform electric field (see Methods). The simulations were performed on a supercell containing $12 \times 1 \times 2$ crystalline unit cells (288 atoms), where periodic boundary conditions were applied in all directions, and a vacuum region of 30 Å was introduced along the $[100]$ direction to remove spurious image interactions (Figure 1a). The PE chain direction is $[001]$, and the simulation cell has 24 PE chains aligned along the $[100]$ direction. We produced a hot electron−hole pair in the middle of a slab at a temperature of 300 K and applied a uniform electric field of $E = 600$ MV/m in the $[100]$ (or x) direction.

We study how the band alignment is affected by applied electric field by calculating the electronic partial density of states (PDOS) projected onto the wave functions of atoms that constitute each PE chain. We show the calculated PDOS without electric field in Figure 1b and that under electric field in Figure 1c. Without electric field (Figure 1b), the PDOS of
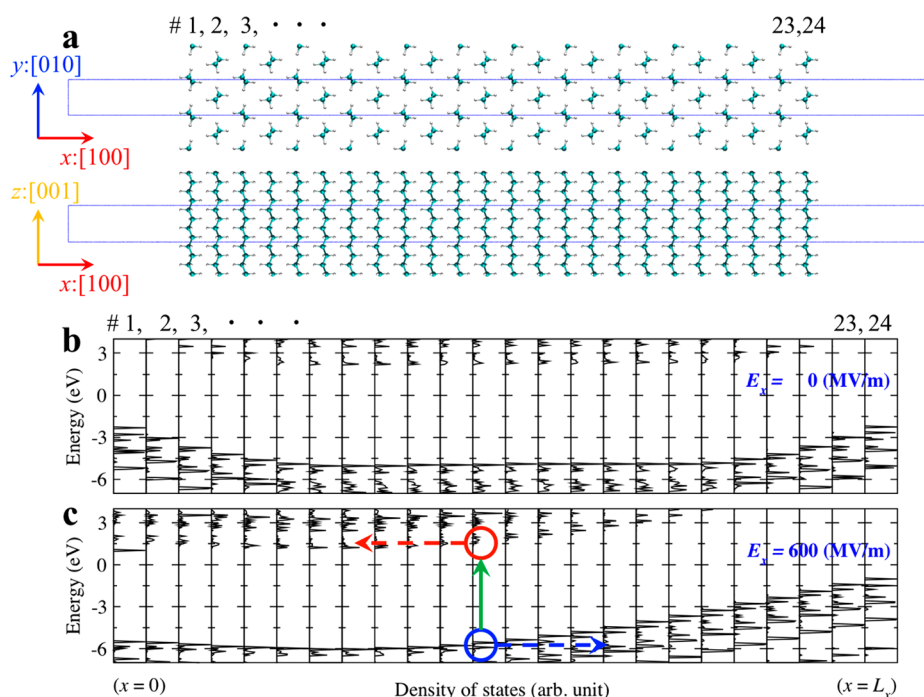
Figure 1. Band alignment in polyethylene. (a) Top and side views of the simulated polyethylene slab with $12 \times 1 \times 2$ unit cells. Carbon and hydrogen atoms are colored in cyan and white, and the blue box shows the simulation cell; atoms outside blue box are image atoms. Polyethylene chains are numbered sequentially starting from $x = 0$ along the x direction. (b and c) Electronic partial densities of states projected onto polyethylene chain under electric field, $E_x = 0$ (b) and 600 MV/m (c). The green arrow indicates an excitation of an electron (red) and hole (blue) pair. The red and blue arrows indicate expected electron and hole movements, respectively, under electric field.
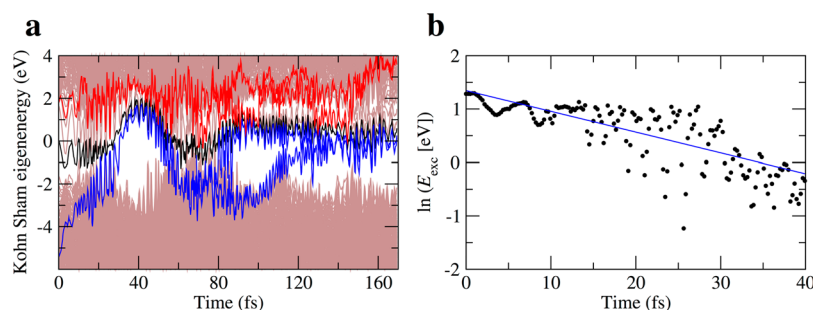

Figure 2. Time evolution of Kohn−Sham eigenenergies. (a) The Kohn−Sham states corresponding to electrons and holes are colored red and blue, respectively. The black line indicates the Fermi energy as a function of time. (b) Semilog plot of the average electronic excitation energy as a function of time, where the blue line indicates an exponential fit.

middle PE chains converge to the bulk behavior, whereas the PDOS of surface PE chains exhibit different behaviors. Namely, both valence band maximum (VBM) and conduction band minimum (CBM) of surface PE chains are higher than those of the bulk, leading to upward bending of the electronic bands at surfaces.[21,22] Under an electric field (Figure 1c), this band bending is superimposed with band tilting due to linear voltage drop. The net effects are a somewhat flat band profile near the lower surface ($x = 0$) versus considerable energy gradient near the upper surface ($x = L_x$), where L_x is the simulation box size in the x direction. In particular, the uppermost (i.e. lowest-voltage) chain #24 has the highest VBM, and the VBM profile near the upper surface reflects a voltage drop, $-x \cdot E_x$. Because a hole under applied electric field (blue circle in Figure 1c) acts as a positive charge $+e$, it is expected to move toward the low-voltage surface, as indicated by the blue arrow in Figure 1c. On the other hand, an excited electron is subjected to little driving force due to a flat CBM

profile near the lower (i.e. high-voltage) surface. As a result, we expect subsequent processes upon electron−hole pair excitation (e.g., formation of defects) are dictated by the hole. The objective of this work is to investigate the formation mechanism of chemical defects. Below, we analyze in detail the elementary processes that eventually lead to defect formation.

Energy Dissipation. We analyzed the dynamics of electrons and holes to understand microscopic mechanisms underlying the dissipation of electronic excitation energy, which in turn gives rise to various subsequent processes. Figure 2a shows time evolution of the Kohn−Sham eigenenergy near the Fermi level. Here, the origin of the energy is the Fermi energy at time $t = 0$, when the excitation takes place. The hole relaxed to the valence band edge rapidly within 20 fs. To quantify the energy loss rate, k, we calculated the average electronic excitation energy
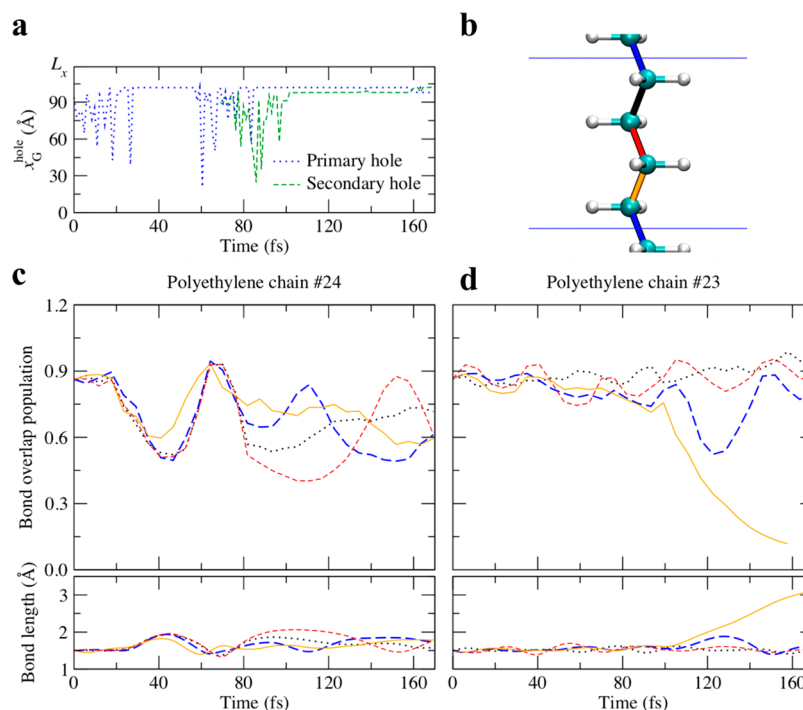
Figure 3. Hole dynamics and change of C−C bond length. (a) Center-of-mass (COM) positions for holes, where the COM positions of chain #23 and #24 are 98.2 and 101.9 Å, respectively. (b) Schematic of the low-voltage surface chains, where white and cyan spheres are H and C atoms, and different C−C bonds are distinguished by different colors (blue, black, red, and orange). (c and d) Bond overlap population between carbon atoms (top) and C−C bond lengths (bottom) in the surface (c) and subsurface (d) chains. The line colors in panels c and d correspond to the bond colors in panel b.

$$
\begin{aligned}
&E_{exc}(t) \\
&= \frac{\sum_i f_i(t)\varepsilon_i(t)\Theta(\varepsilon_i(t)) - \sum_i (1 - f_i(t))\varepsilon_i(t)\Theta(-\varepsilon_i(t))}{\sum_i f_i(t)\Theta(\varepsilon_i(t)) + \sum_i (1 - f_i(t))\Theta(-\varepsilon_i(t))}
\end{aligned}
\tag{1}
$$

where $f_i(t)$ and $\varepsilon_i(t)$ are the occupation number and Kohn−Sham eigenenergy of the ith state as a function of time t, and $\Theta(\varepsilon)$ is the step function. Figure 2b shows the calculated $E_{exc}(t)$ in a semilog plot. The blue line in Figure 2b indicates an exponential decay of the excitation energy, $E_{exc}(t) \propto \exp(-kt)$. The best fit yields $k = (3.9 \pm 0.6) \times 10^{13}$ (s^{-1}). This value is expected to be underestimated, because the noninteracting surface-hopping approach accounts only for electron−phonon interaction.

Within the electron avalanche theory of breakdown in solids, the energy-loss rate k_1 describes the dissipation of electron's energy due to scattering with phonons. This rate is commonly computed as a function of electric field and electron energy, ranging from 0 to the impact ionization threshold, which is of the order of the solid band gap.[7,23−25] Estimation of the energy-dissipation rate shown in Figure 2b instead implies an average over a range of the Kohn−Sham energy. As a comparison, we computed the energy-loss rate of bulk crystalline PE within the density functional perturbation theory (see Methods). By averaging over energy as implied by NAQMD, we obtained $k_1 \approx 1.5 \times 10^{14}$ (s^{-1}). Considering the different geometry (bulk crystal) of this perturbation calculation from that (slab) in the above NAQMD simulation, this rate is consistent with the energy-dissipation rate estimated from the NAQMD simulation.

Carrier Multiplication. Initially at time $t = 0$, only one electron−hole pair existed in our simulation, where the

difference between the electron and hole energies was ∼7 eV (see Figure 2a). Because of nonadiabatic transitions assisted by atomic motions, however, another electron−hole pair was created at 80 fs, leading to carrier multiplication (Figure S1a in the Supporting Information). Just prior to the excitation of the secondary electron−hole pair, the initially hot primary electron−hole pair had been relaxed to near band edges as discussed above. Specifically, the primary electron occupied the lowest unoccupied molecular orbital (LUMO) but three (LUMO+3), while the primary hole occupied the highest occupied molecular orbital (HOMO) but seven (HOMO−7). This primary electron−hole pair caused secondary excitation from HOMO to LUMO+2 (Figure S1b in the Supporting Information). Because unoccupied states near the Fermi level are highly degenerate, the probability of further excitation is high. Movie S1 in the Supporting Information shows the wave functions of both primary and secondary electron−hole pairs. The movie shows that both the primary and secondary holes are driven to the low-voltage surface by an applied electric field.

Defect Formation. We found that the holes, which traveled to the surface, weakened and cleaved C−C bonds. To study the change in C−C bonding, we here focus on the dynamics of holes. The center-of-mass (COM) position of the kth Kohn−Sham wave function in the x direction is computed as

$$
x_G^k = \frac{L_x}{2\pi}\mathrm{Im}\left[\ln\left\{\int_\Omega |\Psi^k(\mathbf{r})|^2 \exp\left(i\frac{2\pi}{L_x}x\right)d\mathbf{r}\right\}\right]
\tag{2}
$$

where $\psi^k(\mathbf{r})$ is the wave function of the kth band and Ω is the volume of the simulation cell. The COM formula, eq 2, is an identity in the spatially localized limit, while satisfying the
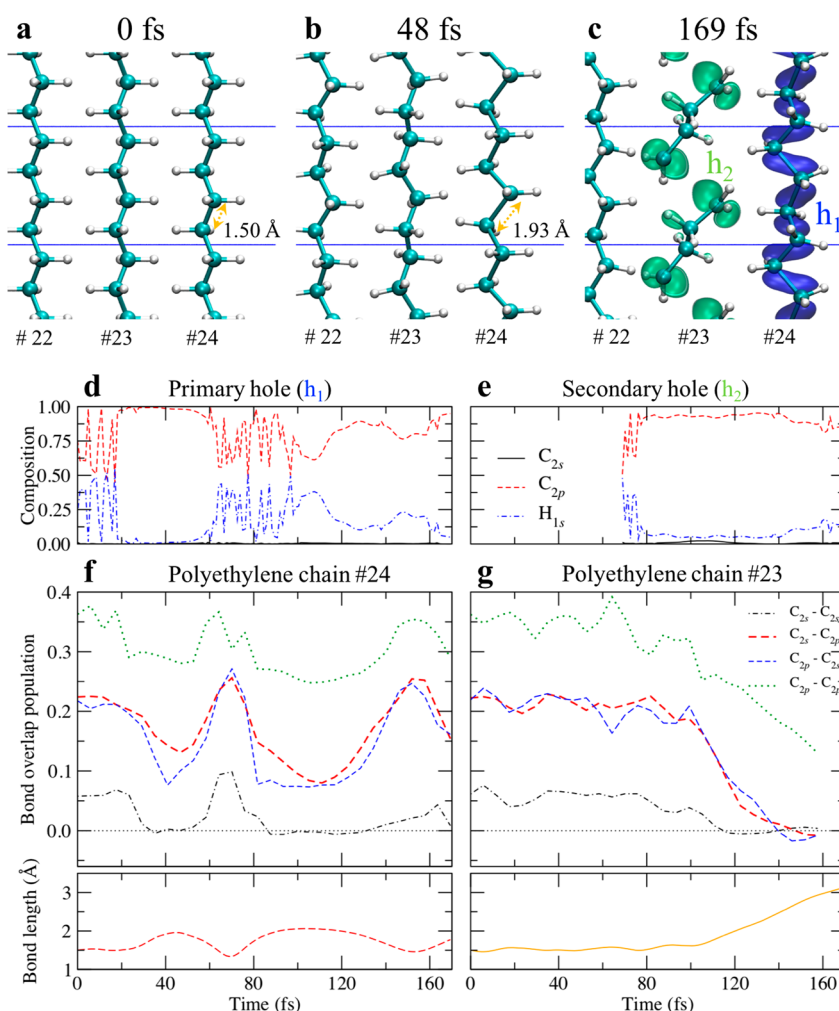
Figure 4. Bond characteristics. (a−c) Snapshots of surface PE chain (#22−#24) at $t = 0$ (a) and 48 fs (b), and the primary (blue) and secondary (green) hole wave functions at 169 fs (c), where the isosurface of 6×10^{-3} a.u.$^{-3}$ is shown. (d and e) Time evolution of the projection of primary-hole (d) and secondary-hole (e) wave functions onto different angular momenta around different atoms. (f and g) Bond overlap population between carbon atoms decomposed by angular momenta (top) and C−C bond length (bottom) of surface (f, #24) and subsurface (g, #23) chains. Here, we focus on the C−C bond colored orange in Figure 3b,c.

periodic boundary condition. Similar formulas have been used for the analysis of electronic wave functions in insulators,[26,27] including the theory of electric polarization.[28,29] Figure 3a shows time evolution of the COM positions of holes. The primary hole was localized on the slab surface (chain #24, see Figure 1) from 30 to 60 fs and after 80 fs, while the secondary hole reached subsurface PE chain (#23) in 100 fs. Namely, both primary and secondary hole states were localized in the lowest-voltage PE chains (#23 or #24) driven by applied electric field. (Hole localization is quantified in terms of the participation number in Figure S2 in the Supporting Information.) This localization of holes on the surface is accompanied by a change of C−C lengths (Figure 3c,d). We observe that C−C bonds in chain #24 were weakened at 48 fs (Figure 3c), while one of the C−C bonds (colored orange) in chain #23 cleaved at 169 fs (Figure 3d).

To quantify change in the bonding properties of atoms, we used bond-overlap population (BOP) analysis[30] by expanding the electronic wave functions in an atomic-orbital basis set. BOP gives a semiquantitative estimate of the strength of covalent bonding between atoms. Panels c and d of Figure 3 show BOP and C−C bond lengths for PE chain #24 (at

surface) and #23 (subsurface), respectively. When a hole was localized in the PE chain #24 (30−60 fs and 80−170 fs; see Figure 3a), C−C bonds became longer and BOP decreased (Figure 3c). However, BOP increased around 60 fs, because a hole was not localized in chain #24 around that time. In chain #23, the effect of localization of holes concentrated on a certain C−C bond (colored orange in Figure 3b), which lead to cleavage of that particular C−C bond (Figure 3d).

To study the electronic character of the holes, we projected their wave functions (Figure 4c) onto different angular momenta around different atoms (Figure 4d,e) and decomposed C−C BOP by angular momenta (Figure 4f,g). Each hole was predominantly composed of 2p orbital of carbon, where the composition of the C-2p orbital was high (∼80%) when a hole reached the slab surface. Moreover, the interaction between s and p orbitals of carbon on PE chain #23 decreased and became zero after a hole reached the slab surface at 100 fs (Figure 4g). Because the C−C bond is a σ bond with sp³ hybrid orbitals, a hole, which takes an electron away from the C-2p orbital, affects the C−C bond. Here, localization of holes is key to the change of C−C bonds. Namely, the VBM is characterized by a C−C σ bond, which is essential to bond the

polymer together, but excited holes weaken it when localized to particular bonds. The resulting defects[14−20] in turn modify charge dynamics,[31] thereby forming a positive feedback loop that leads to dielectric breakdown. While it is difficult to observe these ultrafast processes experimentally, connection with experiments may be established by considering a variety of polymer morphology, defect concentration and location, temperature, and electric-field scenarios, which will be the subject of future studies.

METHODS

Nonadiabatic Quantum Molecular Dynamics. Quantum molecular dynamics (QMD) simulations follow the trajectories of all atoms while computing interatomic forces quantum mechanically from first principles.[32,33] The electronic states were calculated by projector augmented-wave (PAW) method, which is an all-electron electronic structure calculation method within the frozen-core approximation.[34] Projector functions were generated for the 2s and 2p states of carbon and the 1s state of hydrogen. In the framework of density functional theory (DFT),[35,36] the generalized gradient approximation (GGA) was used for the exchange−correlation energy.[37] van der Waals correction was incorporated based on the DFT-D method.[38] The electronic pseudowave functions and pseudo-charge density were expanded by plane waves with cutoff energies of 30 and 300 Ry, respectively. The calculated band gap of bulk PE crystal using these methods (especially GGA) is 6.2 eV, which underestimates an experimental value of 8.8 eV.[39] While this discrepancy may affect the carrier-injection process, subsequent dynamics of hot carriers is likely less sensitive to the band gap. The calculations were performed on a supercell containing $12 \times 1 \times 2$ crystalline unit cells (288 atoms) of polyethylene, where periodic boundary conditions were applied in all directions, and a vacuum region of 30 Å along the x axis was introduced to remove spurious image interactions. Here, each PE crystalline unit cell contains one monomer along the [001] axis (i.e. the chain direction) and two and one polymer chains in the [100] and [010] directions, respectively. The $12 \times 1 \times 2$ supercell (denoted by blue box in Figure 1a) thus contains two monomers in the chain direction, with 24 and 1 chains in the [100] and [010] directions, respectively. The thickness-dependent dielectric response of slabs has been studied intensively, including the existence of dielectric dead layers on slab surfaces.[40] However, thickness-dependent hot-carrier dynamics and chemistry are a much more challenging problem, which defers direct computational study. In order to assess whether the current thickness is sufficient to contain a dielectrically active bulk region instead, we have computed an electrostatic-potential profile. Figure S3 in the Supporting Information plots the local Kohn−Sham potential as a function of x along the [100] direction without (blue) and with (red) an electric field of 600 MV/m. Their difference (black) corresponds to the electric-field contribution. The result shows a clearly delineated slab interior that exhibits linear potential drop (i.e., uniform electric field). Thus, the current simulation satisfactorily represents both dielectrically active bulk crystal (where hot carriers are injected) and surface (where subsequent chemical processes take place). The Γ point was used for Brillouin-zone sampling for electronic-structure calculations. QMD simulations were carried out at a temperature of 300 K in the canonical ensemble using a Nosé−Hoover thermostat. The equations of motion were integrated numerically with a time step of 0.242 fs. We applied a uniform electric field by the linear "sawtooth" potential, i.e., $V_{\text{efield}}(x) = -x \cdot E_x$ ($0 < x < L_x$) in the x direction. To study the dynamics of excited charge carriers, we performed nonadiabatic QMD (NAQMD) simulations.[41−47] The NAQMD method describes electronic excitations in the framework of time-dependent density functional theory (TDDFT).[48] In addition, non-adiabatic transitions between excited electronic states assisted by molecular motions are treated with a surface-hopping approach.[49] The simulations were initiated by exciting one valence-band electron to a conduction-band state, where we choose the valence and conduction states that resided in the center of the slab so as to simulate bulk hot-carrier generation. Here, we have used a simple initial condition consisting of a single electron−hole pair placed in the middle of the slab, similar to our previous work.[50] While this approach neglects attosecond carrier-injection dynamics[51] and the complexity of carrier-injection processes likely at polymer−electrode interfaces, it suffices to describe subsequent carrier dynamics, electron−phonon scattering, and chemistry in 1−100 fs, which is the focus of this Letter. We used our own QMD simulation code implemented on massively parallel computers.[52]

Quantum-Mechanical Perturbation Calculation. The electron energy-loss rate k_l was evaluated using quantum-mechanical perturbation calculations within the theory of electron-avalanche breakdown in solids.[7,23] The energy-loss rate, which describes the energy exchange of the electron scattering from the (wave vector and band index) initial state ($\mathbf{k}j$) to the final state ($\mathbf{k} + \mathbf{q}j'$) involving a phonon at state ($\mathbf{q}, \lambda$) is given by[7,23]

$$k_l(\mathcal{E}) = \frac{2\pi}{D(\mathcal{E})} \sum_{\pm} \sum_{\mathbf{k}j} \sum_{\mathbf{q}\lambda j'} \left\{ \pm \omega_{\mathbf{q}\lambda} |g^{\mathbf{q}\lambda}_{\mathbf{k}+\mathbf{q}j',\mathbf{k}j}|^2 \left(n_{\mathbf{q}\lambda} + \frac{1}{2} \mp \frac{1}{2} \right) \right.$$
$$\left. \delta(\varepsilon_{\mathbf{k}j} - \varepsilon_{\mathbf{k}+\mathbf{q}j'} \pm \hbar\omega_{\mathbf{q}\lambda}) \delta(\varepsilon_{\mathbf{k}j} - \mathcal{E}) \right\} \quad (3)$$

Here, $\hbar$ is the reduced Planck's constant, $\mathcal{E}$ the electron energy referenced to the valence band minimum, and $D(\mathcal{E})$ the electronic density of states; $\omega_{\mathbf{q}\lambda}$ and $n_{\mathbf{q}\lambda}$ are the phonon frequency and occupation number at state ($\mathbf{q}\lambda$), respecively; $\varepsilon_{\mathbf{k}j}$ and $\varepsilon_{\mathbf{k}+\mathbf{q}j'}$ are the electron energy at the initial and final states, respectively. The electron−phonon coupling $g^{\mathbf{q}\lambda}_{\mathbf{k}+\mathbf{q}j',\mathbf{k}j}$ has been computed[23−25] within the density functional perturbation theory as implemented in the Quantum ESPRESSO code.[53]

ASSOCIATED CONTENT

Ⓢ Supporting Information

The Supporting Information is available free of charge on the ACS Publications website at DOI: 10.1021/acs.jpclett.9b01344.

> Detailed analysis of carrier multiplication and localization (PDF).
>
> Video showing the dynamics of electron and hole wave functions represented by red and blue isosurfaces, respectively; time evolution of Kohn−Sham eigenenergies (magenta lines), where excited electrons and holes are denoted by red and blue dots, respectively (MP4)

AUTHOR INFORMATION

Corresponding Author

*E-mail: anakano@usc.edu.

ORCID

Chiho Kim: 0000-0002-1814-4980
Tran Doan Huan: 0000-0002-8093-9426
Aiichiro Nakano: 0000-0003-3228-3896
Rampi Ramprasad: 0000-0003-4630-1565
Priya Vashishta: 0000-0003-4683-429X

Author Contributions

Notes

The authors declare no competing financial interest.

■ ACKNOWLEDGMENTS

■ REFERENCES

(1) Zhang, Q. M.; Bharti, V.; Zhao, X. Giant electrostriction and relaxor ferroelectric behavior in electron-irradiated poly(vinylidene fluoride-trifluoroethylene) copolymer. *Science* **1998**, *280*, 2101−2104.

(2) Chu, B. J.; Zhou, X.; Ren, K. L.; Neese, B.; Lin, M. R.; Wang, Q.; Bauer, F.; Zhang, Q. M. A dielectric polymer with high electric energy density and fast discharge speed. *Science* **2006**, *313*, 334−336.

(3) Sharma, V.; Wang, C. C.; Lorenzini, R. G.; Ma, R.; Zhu, Q.; Sinkovits, D. W.; Pilania, G.; Oganov, A. R.; Kumar, S.; Sotzing, G. A.; Boggs, S. A.; Ramprasad, R. Rational design of all organic polymer dielectrics. *Nat. Commun.* **2014**, *5*, 4845.

(4) Su, H. B.; Strachan, A.; Goddard, W. A. Density functional theory and molecular dynamics studies of the energetics and kinetics of electroactive polymers: PVDF and P(VDF-TrFE). *Phys. Rev. B: Condens. Matter Mater. Phys.* **2004**, *70*, 064101.

(5) Ieda, M. Dielectric breakdown process of polymers. *IEEE Trans. Ele.c Insul.* **1980**, *15*, 206−224.

(6) Jones, J. P.; Llewellyn, J. P.; Lewis, T. J. The contribution of field-induced morphological change to the electrical aging and breakdown of polyethylene. *IEEE Trans. Dielectr. Electr. Insul.* **2005**, *12*, 951−966.

(7) Sparks, M.; Mills, D. L.; Warren, R.; Holstein, T.; Maradudin, A. A.; Sham, L. J.; Loh, E.; King, D. F. Theory of electron-avalanche breakdown in solids. *Phys. Rev. B: Condens. Matter Mater. Phys.* **1981**, *24*, 3519−3536.

(8) Sun, Y.; Bealing, C.; Boggs, S.; Ramprasad, R. 50+ years of intrinsic breakdown. *IEEE Elec. Insu.l Mag.* **2013**, *29*, 8−15.

(9) Zener, C. A theory of the electrical breakdown of solid dielectrics. *Proc. R. Soc. London, Ser. A* **1934**, *145*, 523−529.

(10) Fröhlich, A. Theory of electrical breakdown in ionic crystals. *Proc. R. Soc. A* **1937**, *160*, 230−241.

(11) Von Hippel, A. Electric breakdown of solid and liquid insulators. *J. Appl. Phys.* **1937**, *8*, 815−832.

(12) Bealing, C. R.; Ramprasad, R. An atomistic description of the high-field degradation of dielectric polyethylene. *J. Chem. Phys.* **2013**, *139*, 174904.

(13) Righi, M. C.; Scandolo, S.; Serra, S.; Iarlori, S.; Tosatti, E.; Santoro, G. Surface states and negative electron affinity in polyethylene. *Phys. Rev. Lett.* **2001**, *87*, 076802.

(14) Meunier, M.; Quirke, N.; Aslanides, A. Molecular modeling of electron traps in polymer insulators: chemical defects and impurities. *J. Chem. Phys.* **2001**, *115*, 2876−2881.

(15) Chen, L. H.; Tran, H. D.; Wang, C. C.; Ramprasad, R. Unraveling the luminescence signatures of chemical defects in polyethylene. *J. Chem. Phys.* **2015**, *143*, 124907.

(16) Chen, L. H.; Huan, T. D.; Ramprasad, R. Electronic structure of polyethylene: role of chemical, morphological and interfacial complexity. *Sci. Rep.* **2017**, *7*, 6128.

(17) Chen, L. H.; Tran, H. D.; Ramprasad, R. Atomistic mechanisms for chemical defects formation in polyethylene. *J. Chem. Phys.* **2018**, *149*, 234902.

(18) Meunier, M.; Quirke, N. Molecular modeling of electron trapping in polymer insulators. *J. Chem. Phys.* **2000**, *113*, 369−376.

(19) Cubero, D.; Quirke, N. Computer simulations of localized small polarons in amorphous polyethylene. *J. Chem. Phys.* **2004**, *120*, 7772−7778.

(20) Moyassari, A.; Unge, M.; Hedenqvist, M. S.; Gedde, U. W.; Nilsson, F. First-principle simulations of electronic structure in semicrystalline polyethylene. *J. Chem. Phys.* **2017**, *146*, 204901.

(21) Zhang, Z.; Yates, J. T. Band bending in semiconductors: chemical and physical consequences at surfaces and interfaces. *Chem. Rev.* **2012**, *112*, 5520−5551.

(22) Kwon, S. K.; Nabi, Z.; Kadas, K.; Vitos, L.; Kollar, J.; Johansson, B.; Ahuja, R. Surface energy and stress release by layer relaxation. *Phys. Rev. B: Condens. Matter Mater. Phys.* **2005**, *72*, 235423.

(23) Sun, Y.; Boggs, S. A.; Ramprasad, R. The intrinsic electrical breakdown strength of insulators from first principles. *Appl. Phys. Lett.* **2012**, *101*, 132906.

(24) Kim, C.; Pilania, G.; Ramprasad, R. From organized high-throughput data to phenomenological theory using machine learning: the example of dielectric breakdown. *Chem. Mater.* **2016**, *28*, 1304−1311.

(25) Kim, C.; Ramprasad, R. Dielectric breakdown field of strained silicon under hydrostatic pressure. *Appl. Phys. Lett.* **2017**, *111*, 112904.

(26) Kohn, W. Theory of insulating state. *Phys. Rev.* **1964**, *133*, A171−A181.

(27) Hakamata, T.; Shimamura, K.; Shimojo, F.; Kalia, R. K.; Nakano, A.; Vashishta, P. The nature of free-carrier transport in organometal halide perovskites. *Sci. Rep.* **2016**, *6*, 19599.

(28) Resta, R. Quantum-mechanical position operator in extended systems. *Phys. Rev. Lett.* **1998**, *80*, 1800−1803.

(29) Umari, P.; Pasquarello, A. Ab initio molecular dynamics in a finite homogeneous electric field. *Phys. Rev. Lett.* **2002**, *89*, 157602.

(30) Mulliken, R. S. Electronic population analysis on LCAO-MO molecular wave functions. 1. *J. Chem. Phys.* **1955**, *23*, 1833−1840.

(31) Sun, L. X.; Marrocchelli, D.; Yildiz, B. Edge dislocation slows down oxide ion diffusion in doped CeO_2 by segregation of charged defects. *Nat. Commun.* **2015**, *6*, 6294.

(32) Car, R.; Parrinello, M. Unified approach for molecular-dynamics and density-functional theory. *Phys. Rev. Lett.* **1985**, *55*, 2471−2474.

(33) Payne, M. C.; Teter, M. P.; Allan, D. C.; Arias, T. A.; Joannopoulos, J. D. Iterative minimization techniques for ab initio total-energy calculations - molecular-dynamics and conjugate gradients. *Rev. Mod. Phys.* **1992**, *64*, 1045−1097.

(34) Blochl, P. E. Projector augmented-wave method. *Phys. Rev. B: Condens. Matter Mater. Phys.* **1994**, *50*, 17953−17979.

(35) Hohenberg, P.; Kohn, W. Inhomogeneous electron gas. *Phys. Rev.* **1964**, *136*, B864−B871.

(36) Kohn, W.; Sham, L. J. Self-consistent equations including exchange and correlation effects. *Phys. Rev.* **1965**, *140*, A1133−A1138.

(37) Perdew, J. P.; Burke, K.; Ernzerhof, M. Generalized gradient approximation made simple. *Phys. Rev. Lett.* **1996**, *77*, 3865−3868.

(38) Grimme, S. Semiempirical GGA-type density functional constructed with a long-range dispersion correction. *J. Comput. Chem.* **2006**, *27*, 1787−1799.

(39) Less, K. J.; Wilson, E. G. Intrinsic photoconduction and photoemission in polyethylene. *J. Phys. C: Solid State Phys.* **1973**, *6*, 3110−3121.

(40) Stengel, M.; Spaldin, N. A. Origin of the dielectric dead layer in nanoscale capacitors. *Nature* **2006**, *443*, 679−682.

(41) Craig, C. F.; Duncan, W. R.; Prezhdo, O. V. Trajectory surface hopping in the time-dependent Kohn-Sham approach for electron-nuclear dynamics. *Phys. Rev. Lett.* **2005**, *95*, 163001.

(42) Meng, S.; Kaxiras, E. Real-time, local basis-set implementation of time-dependent density functional theory for excited state dynamics simulations. *J. Chem. Phys.* **2008**, *129*, 054110.

(43) Shimojo, F.; Ohmura, S.; Mou, W.; Kalia, R. K.; Nakano, A.; Vashishta, P. Large nonadiabatic quantum molecular dynamics simulations on parallel computers. *Comput. Phys. Commun.* **2013**, *184*, 1−8.

(44) Imachi, H.; Yokoyama, S.; Kaji, T.; Abe, Y.; Tada, T.; Hoshi, T. One-hundred-nm-scale electronic structure and transport calculations of organic polymers on the K computer. *AIP Conf. Proc.* **2016**, *1790*, 020010.

(45) Lin, M. F.; Kochat, V.; Krishnamoorthy, A.; Bassman, L.; Weninger, C.; Zheng, Q.; Zhang, X.; Apte, A.; Tiwary, C. S.; Shen, X. Z.; Li, R. K.; Kalia, R.; Ajayan, P.; Nakano, A.; Vashishta, P.; Shimojo, F.; Wang, X. J.; Fritz, D. M.; Bergmann, U. Ultrafast non-radiative dynamics of atomically thin $MoSe_2$. *Nat. Commun.* **2017**, *8*, 1745.

(46) Bassman, L.; Krishnamoorthy, A.; Kumazoe, H.; Misawa, M.; Shimojo, F.; Kalia, R. K.; Nakano, A.; Vashishta, P. Electronic origin of optically-induced sub-picosecond lattice dynamics in $MoSe_2$ monolayer. *Nano Lett.* **2018**, *18*, 4653−4658.

(47) Tung, I.; Krishnamoorthy, A.; Sadasivam, S.; Zhou, H.; Zhang, Q.; Seyler, K. L.; Clark, G.; Mannebach, E. M.; Nyby, C.; Ernst, F.; Zhu, D.; Glownia, J. M.; Kozina, M. E.; Song, S.; Nelson, S.; Kumazoe, H.; Shimojo, F.; Kalia, R. K.; Vashishta, P.; Darancet, P.; Heinz, T. F.; Nakano, A.; Xu, X.; Lindenberg, A. M.; Wen, H. Anisotropic structural dynamics of monolayer crystals revealed by femtosecond surface x-ray scattering. *Nat. Photonics* **2019**, *13*, 425−430.

(48) Runge, E.; Gross, E. K. U. Density-functional theory for time-dependent systems. *Phys. Rev. Lett.* **1984**, *52*, 997−1000.

(49) Tully, J. C. Molecular dynamics with electronic transitions. *J. Chem. Phys.* **1990**, *93*, 1061−1071.

(50) Brown, E.; Sheng, C.; Shimamura, K.; Shimojo, F.; Nakano, A. Enhanced charge recombination due to surfaces and twin defects in GaAs nanostructures. *J. Appl. Phys.* **2015**, *117*, 054307.

(51) Sommer, A.; Bothschafter, E. M.; Sato, S. A.; Jakubeit, C.; Latka, T.; Razskazovskaya, O.; Fattahi, H.; Jobst, M.; Schweinberger, W.; Shirvanyan, V.; Yakovlev, V. S.; Kienberger, R.; Yabana, K.; Karpowicz, N.; Schultze, M.; Krausz, F. Attosecond nonlinear polarization and light-matter energy transfer in solids. *Nature* **2016**, *534*, 86−90.

(52) Shimojo, F.; Hattori, S.; Kalia, R. K.; Kunaseth, M.; Mou, W.; Nakano, A.; Nomura, K.-i.; Ohmura, S.; Rajak, P.; Shimamura, K.; Vashishta, P. A divide-conquer-recombine algorithmic paradigm for multiscale materials modeling. *J. Chem. Phys.* **2014**, *140*, 18A529.

(53) Giannozzi, P.; Baroni, S.; Bonini, N.; Calandra, M.; Car, R.; Cavazzoni, C.; Ceresoli, D.; Chiarotti, G. L.; Cococcioni, M.; Dabo, I.; Dal Corso, A.; de Gironcoli, S.; Fabris, S.; Fratesi, G.; Gebauer, R.; Gerstmann, U.; Gougoussis, C.; Kokalj, A.; Lazzeri, M.; Martin-Samos, L.; Marzari, N.; Mauri, F.; Mazzarello, R.; Paolini, S.; Pasquarello, A.; Paulatto, L.; Sbraccia, C.; Scandolo, S.; Sclauzero, G.; Seitsonen, A. P.; Smogunov, A.; Umari, P.; Wentzcovitch, R. M. QUANTUM ESPRESSO: a modular and open-source software project for quantum simulations of materials. *J. Phys.: Condens. Matter* **2009**, *21*, 395502.